

## NUMERICAL SIMULATION AND EXPERIMENTAL RESEARCH OF MULTI-PIPE JET FIREBALL

by

**Bin TAI<sup>a,b</sup>, and Xiaojian HAO<sup>a,b\*</sup>**

<sup>a</sup>Science and Technology on Electronic Test and Measurement Laboratory,  
North University of China, Taiyuan Shanxi Province, China

<sup>b</sup>School of Instrument and Electronics, North University of China, Taiyuan, China

Original scientific paper

<https://doi.org/10.2298/TSCI220129090T>

*This paper studies a self-designed high temperature fireball quasi-static simulation device to understand the temperature distribution of each substance inside the fireball under the multi-pipe injection technology. The changes in the physical field of the high temperature fireball are obtained through numerical simulation. The simulation model in this paper adopts the turbulent k- $\epsilon$  model, and simulates the material transfer process according to Fick's law. The commercial software COMSOL multiphysics is used to give and analyze the local characteristics of fluid-flow and heat transfer. The simulation device formed a high temperature fireball under the interaction of the three-way jet fire. The experimental data verified the accuracy of the simulation results, and the experimental results were in good agreement with the simulation results. This method of analyzing the actual temperature field through simulation can be used to provide a powerful verification scheme for the detection of complex multi-temperature fields in the future.*

**Key words:** *simulation device, numerical simulation, high temperature fireball, data analysis*

### Introduction

Due to the influence of extreme environment such as high temperature, high pressure, high speed and high impact, it is difficult to measure the transient high temperature of high temperature fireball in the explosion scene accurately. This kind of transient temperature measurement is often accompanied by high pressure or high-speed air-flow, most of which are non-repeatable one-time processes. Therefore, the problems of poor measurement conditions, high technical difficulty and inaccurate temperature measurement cannot be ignored. At the same time, the reliability of the system and data acquisition speed are also required. In this paper, a numerical simulation method is proposed to simulate the artificial fireball to verify the accuracy of the simulation, which provides a new idea for the detection of complex multi physical fields. The combustion of fireball includes various physical phenomena, such as fluid-flow, fluid heat transfer and chemical reaction, and so on. Due to the complexity of multi pipe injection technology and the influence of simulation device and experimental environment, it is very difficult to analyze the fluid-flow and heat transfer in fireball by experiment.

---

\*Corresponding author, e-mail: haoxiaojian@nuc.edu.cn

Although many temperature sensors are suitable for different temperature range and response speed, the theoretical research and practice of temperature measurement cannot meet the needs of measurement work. This paper proposes a simulation verification method based on multi-pipe injection technology, combined with multi-physics simulation and parallel control technology to study the multi-physical characteristics of explosive fireballs. Through the numerical analysis and modeling simulation of the research object, the numerical analysis of 3-D flame propagation [1], the CFD model analysis of gas-solid two-phase flow in the flow chamber [2, 3], the temperature distribution analysis [4], and particle characteristics analysis of high temperature flame spraying [5, 6] are carried out, which provides a strong theoretical basis for the design of experimental verification method for simulating high temperature fireball. Wang *et al.* [7] used a fully developed axisymmetric turbulent pipe flow to simulate flame. The experimental configuration was a circular premixed methane air burner operating at atmospheric pressure. Gonzalez *et al.* [8] used commercial CFD software ANSYS FLUENT to model the fluid-flow and heat transfer of industrial boilers. Lan *et al.* [9] established a numerical model for the combustion of an ethylene furnace to analyze the fluid-flow and heat transfer in the furnace. Zhang *et al.* [10] of Harbin Engineering University used the eddy dissipation concept model to simulate the 3-D turbulent combustion flow field in the plasma generator. According to the spectral characteristics of flame high temperature field, Professor Zhou Huaichun [11] led a team in Huazhong University of science and technology to reasonably select and simplify the radiation transfer model, and combined with spectral analysis and radiation temperature measurement technology to reconstruct the 2-D spectral emissivity and temperature field of flame. Collazo *et al.* [12] used numerical models to simulate wood combustion. They compared the numerical results with the experimental results, and the results showed good consistency. Through a 3-D numerical model, Gomez *et al.* [13] verified the consistency between the numerical simulation results and the experimental results of the biomass packed bed combustion behavior. The validity of the numerical model is verified by comparing the numerical simulation with the experiment. In order to check the combustion of propane, Hjartstam *et al.* [14] carried out various CFD simulations. Ghadamgahi *et al.* [15] used CFD method to simulate combustion under different turbulence models. Khare *et al.* [16] proposed the CFD simulation of oxygen coal pilot scale combustion. Wang *et al.* [17] used many results from the literature at that time to conduct a parametric numerical simulation study on the propane furnace. Liu *et al.* [18] studied the effects of initial parameters on combustion and emission of homogeneous charge compression ignition by using the coupled 3-D CFD and detailed chemical kinetic model of free piston engine generator. Samal *et al.* [19] studied the influence of turbulence model on the efficiency of gas turbine combustor. Through theoretical research and mathematical software modeling, they provided a design solution to significantly improve the efficiency and reliability of gas turbine combustor. Kun *et al.* [20] used hidden temperature method to solve the temperature field model and artificial neural network to establish the corresponding relationship of node temperature values in the iterative process. Wang *et al.* [21] conducted CFD simulation on the natural gas emission in the sidewall burner. Using the simulation results, the emission of  $\text{NO}_x$  was successfully reduced and the combustion performance of natural gas was improved. Xie *et al.* [22] independently designed a small diesel burner with self-circulating flue gas and studied it using numerical calculation method to analyze the long flame and high pollution emissions of the low-power burner. Therefore, the method based on numerical simulation has been widely used to analyze the temperature distribution of combustion. Numerical simulation has proved to be a powerful and cost-effective engineering tool although the measurement of experimental results will be limited.

Because the formation of explosion fireball is too short, the experimental data is not enough to clearly understand the fluid situation and temperature distribution in the fireball. Therefore, in order to obtain better results, it is necessary to change some conditions to achieve a stab. High temperature fireball which can be tested in the laboratory environment. In order to complete this project, a quasi-static simulation device of high temperature fireball is designed to generate a stable fireball, and numerical simulation is carried out on the environment under the multi pipe injection technology in order to understand the flow field and temperature distribution inside the fireball. Oxyacetylene flame is used as the fire source, and a stable fireball is formed by multi pipeline injection technology. This study uses Fick's law to model mass transport, which is simulated by the turbulent  $k-\varepsilon$  model in the commercial software COMSOL Multiphysics. By comparing the simulation results with the experimental results, we can successfully analyze the flow field and temperature distribution in the fireball.

### Experimental device

The geometric structure of high temperature fireball quasi-static simulation device is shown in fig. 1. According to the function relationship between nozzle center and multi-physical characteristics, the state of three groups of nozzles is automatically controlled by manually set multi-physical field parameters and realized the automatic control of multi-physical field of simulated fireball. High temperature gas is injected by multi pipeline injection technology, as shown in fig. 2, forming a 3-D high temperature flame area meeting the experimental requirements.



Figure 1. Simulation device diagram

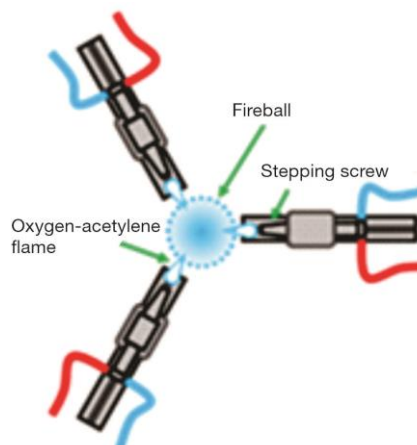


Figure 2. Schematic diagram of multi pipe jet fireball

Oxyacetylene flame was used as fire source to form high temperature fireball. When the mixing ratio of oxygen and acetylene is 1-1.3, the flame produced is called neutral flame. It is composed of flame core, inner flame and outer flame: the flame core near the welding nozzle is white and bright, and the temperature is about 800-1200 °C. The second is the inner flame, which is blue purple. Its temperature range is 2800-3200 °C, and the highest temperature is 2-4 mm away from the tip of the flame core, which can reach 3100-3200 °C. The outer layer is the outer flame, which is orange red. The temperature is about 1200-2500 °C, which is lower than the core and inner flame [23].

### Numerical simulation

In the simulation, the environment area where the three sets of spray guns and fireballs are located is taken as the calculation domain, as shown in fig. 3. In order to get the best simulation result quality in each simulation, we select the more refined grid to divide the model, as shown in fig. 4.



Figure 3. Model diagram

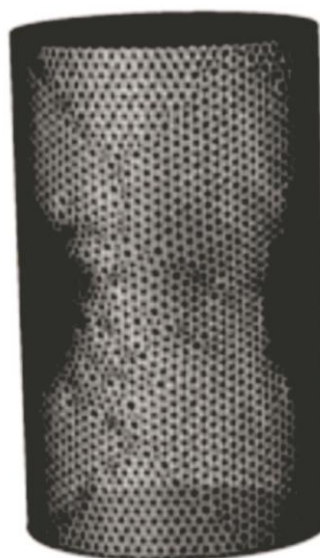


Figure 4. Gridding graph

### Turbulence model

In order to approach a more realistic flame effect, it is necessary to analyze the fluid state of the flame:

$$\text{Re} = \frac{\rho UL}{\mu} \quad (1)$$

where  $\mu$  is the dynamic viscosity,  $\rho$  – the density, and  $U$  and  $L$  are the velocity and length scales of turbulence respectively.

The Reynolds number of the jet is about 29625, which indicates that the jet is turbulent.

Navier-Stokes equations can be used for turbulence simulation, although this will require a large number of elements to capture the various scales in the flow.

The weakly compressible Navier-Stokes equation takes the following form:

$$\rho \frac{\partial \mathbf{u}}{\partial t} + \rho(\mathbf{u} \nabla) \mathbf{u} = \nabla[-p\mathbf{I} + \mathbf{K}] + \mathbf{F} \quad (2)$$

$$\mathbf{K} = (\mu + \mu_\tau) [\nabla \mathbf{u} + (\nabla \mathbf{u})^T] - \frac{2}{3} (\mu + \mu_\tau) (\nabla \mathbf{u}) \mathbf{I} - \frac{2}{3} \rho k \mathbf{I} \quad (3)$$

where  $\rho$  is the density,  $\mathbf{u}$  – the velocity field,  $p$  – the pressure,  $\mu$  – the dynamic viscosity,  $T$  – the absolute temperature, and  $\mathbf{F}$  – the turbulent stress.

The separation method is used to solve the turbulence [24]: one is Navier- Stokes equations, the other is turbulent transport equations.

The turbulence viscosity is modeled:

$$\mu_T = \rho C_\mu \frac{k^2}{\varepsilon} \quad (4)$$

where  $\mu_T$  is the eddy viscosity and  $C_\mu$  is a model constant.

Then the conditions are:

$$P_k = \mu_T \left( \nabla \mathbf{u} : \left[ \nabla \mathbf{u} + (\nabla \mathbf{u})^T \right] - \frac{2}{3} (\nabla \mathbf{u})^2 \right) - \frac{2}{3} \rho k \nabla \mathbf{u} \quad (5)$$

The transport equation of turbulent kinetic energy  $K$  is as follows:

$$\rho \frac{\partial k}{\partial t} + \rho \mathbf{u} \nabla k = \nabla \cdot \left[ \left( \mu + \frac{\mu_T}{\sigma_k} \right) \nabla k \right] + P_k - \rho \varepsilon \quad (6)$$

The transport equation of turbulent dissipation rate  $\varepsilon$  is as:

$$\rho \frac{\partial \varepsilon}{\partial t} + \rho \mathbf{u} \nabla \varepsilon = \nabla \cdot \left[ \left( \mu + \frac{\mu_T}{\sigma_\varepsilon} \right) \nabla \varepsilon \right] + C_{\varepsilon 1} \frac{\varepsilon}{k} P_k - C_{\varepsilon 2} \rho \frac{\varepsilon^2}{k} \quad (7)$$

The model parameters [25] in formula (4)-(7) are listed in tab. 1.

**Table 1. Model parameter**

$C_\mu$	0.09
$C_{\varepsilon 1}$	1.44
$C_{\varepsilon 2}$	1.92
$\sigma_k$	1.0
$\sigma_\varepsilon$	1.3

### Heat transfer model

The fluid heat transfer interface is solved by equation [26]:

$$\rho C_p \left( \frac{\partial T}{\partial t} + \mathbf{u} \nabla T \right) + \nabla \cdot (q + q_r) = a_p T \left( \frac{\partial p}{\partial t} + \mathbf{u} \nabla p \right) + \boldsymbol{\tau} : \nabla \mathbf{u} + Q \quad (8)$$

where  $\rho$  is the density,  $C_p$  – the specific heat capacity under constant pressure,  $T$  – the absolute temperature,  $\mathbf{u}$  – the velocity vector, and  $q$  – the heat transfer flux. When the turbulence model is used in the flow interface, the heat flux is defined as:

$$q = -(k + k_T) \nabla T \quad (9)$$

where  $k$  is the Boltzmann constant,  $k_T$  – the turbulent thermal conductivity,  $q_r$  – the radiant heat flux,  $p$  – the pressure,  $\boldsymbol{\tau}$  – the viscous stress tensor,  $Q$  – includes the heat source other than viscous dissipation, and  $a_p$  – the coefficient of thermal expansion:

$$a_p = -\frac{1}{\rho} \frac{\partial \rho}{\partial T} \quad (10)$$

For ideal gases, the thermal expansion coefficient takes a simpler form:

$$a_p = \frac{1}{T} \quad (11)$$

### Numerical results and experimental analysis

In order to ensure the accuracy of the simulation under the multi pipe injection technology, the numerical simulation of the jet flame of the single spray gun is carried out. fig. 5 depicts the temperature distribution of the flame in a single spray gun after the jet is stabilized. It can be observed that the acetylene flame is fully combusted under the chemical reaction of the concentrated substances. The temperature reaches the maximum value at first near the nozzle, and then decreases gradually with the outward diffusion of the fluid flame.

In order to be able to more clearly sense the temperature of the flame jet, fig. 6 depicts the temperature curve at the radial distance of the nozzle. As can be seen from fig. 6, the maximum temperature of the flame exceeds 3000 °C, reaching about 3100 °C.

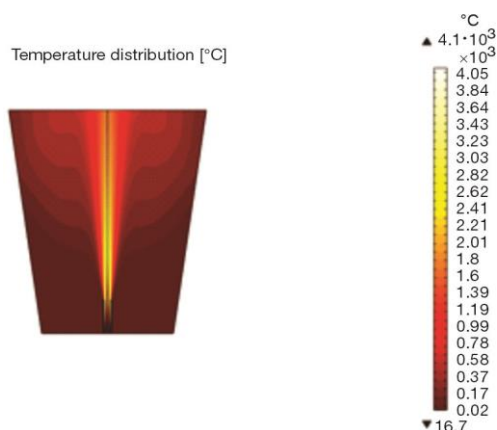


Figure 5. Temperature of single spray gun

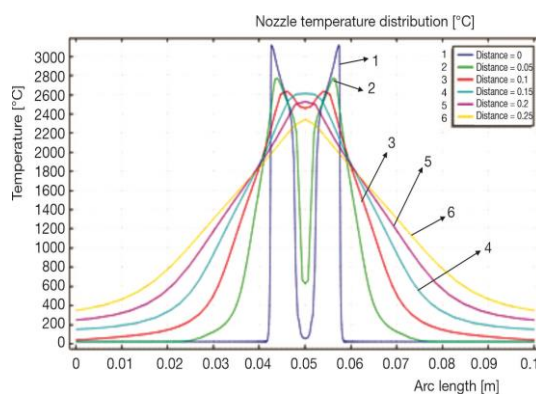


Figure 6. Radial temperature of nozzle

The temperature of full combustion of acetylene and oxygen in the single spray gun is more than 3000 °C, which basically meets the temperature range of explosion field. On this basis, the temperature field under the action of two spray guns is explored.

After the simulation results come out, a simple cross-sectional analysis is carried out on the results of the two spray guns. As shown in fig. 7, the flames of the two spray guns first converge at the center in fig. 7(a). Under the cross action at the center, a large amount of flame is sprayed to the center of the superior arc of the circle where the two spray guns are located, and a small part is sprayed to the center of the minor arc in fig. 7(b).

Then the temperature section is drawn. It is also easy to see from the temperature section in fig. 8 that most of the flames are concentrated in the arc. The temperature data is derived and the curve shown in fig. 9 is drawn.

It can be seen from the fig. 9 that the temperature range of the two spray guns varies greatly. Close to the center, the maximum temperature is only 2600 °C, which cannot meet the 3000 °C that can be reached in general explosion places for the time being. Therefore, three sets of spray guns are used to carry out the simulation study under multi-pipe injection.

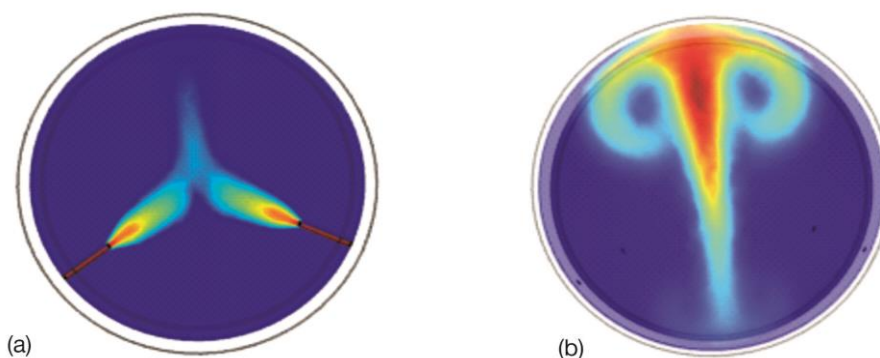


Figure 7. Schematic diagram of two way spray gun

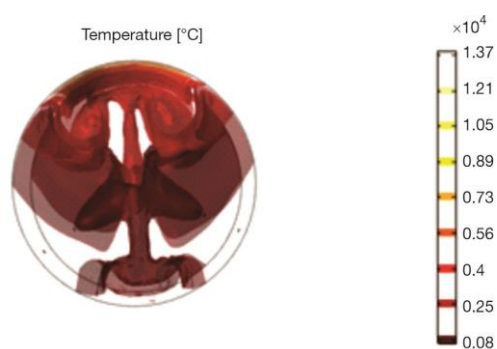


Figure 8. Temperature distribution

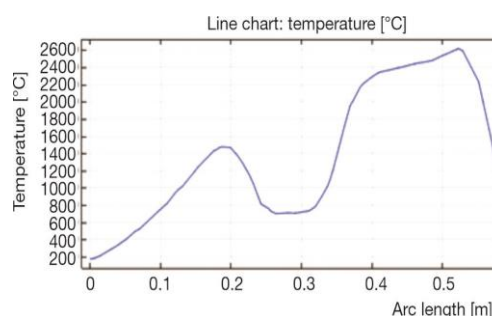


Figure 9. Temperature graph

In each numerical simulation, the simulation results are closely related to the meshing situation. Under normal circumstances, the best simulation results can be obtained by choosing a very fine mesh, but the increase in mesh quality will also lead to a significant increase in simulation time and running memory. Therefore, three kinds of grids are analyzed in the case of multi-pipe injection simulation. The grid characteristics are shown in the tab. 2.

Table 2. Mesh characteristics

	First mesh	Second mesh	Third mesh
Number of grid cells	287888	1190413	4262318
Minimum unit quality	0.09321	0.1459	0.1754
Average unit quality	0.6619	0.6627	0.6623
Mesh vertex	50274	204404	723182

According to the generated results of the mesh quality, the effect of the generated mesh on the temperature distribution can be observed. For the first mesh, the temperature distribution is given, as shown in fig. 10. Obviously, the sparse grid will lead to large errors in temperature distribution, so the result of the first grid is directly excluded.

In the simulation process, the relative error tolerance is 0.01 and the number of iterations is 300. In order to make the data representative and accurate, the second grid is taken as an example to analyze the different relative error tolerance and iteration times. Fill in the collected temperature data in tab. 3.

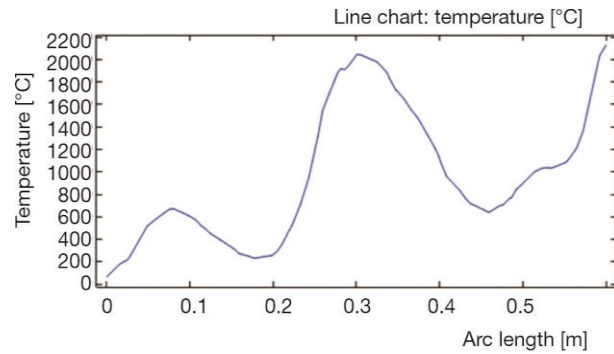


Figure. 10 The first mesh temperature graph

Table 3. Dissimilar error iteration data

Arc length [m]	Relative error tolerance: 0.01 Number of iterations: 300	Relative error tolerance: 0.005 Number of iterations: 300	Relative error tolerance: 0.001 Number of iterations: 1000
0.260	1124.6	1124.7	1124.7
0.273	1853.7	1853.7	1853.6
0.290	2624.8	2624.8	2624.8
0.303	2984.6	2984.7	2984.6
0.315	3034.3	3034.3	3034.4
0.328	2855.6	2855.7	2855.7
0.341	2468.5	2468.6	2468.6
0.354	2097.8	2097.9	2097.8
0.366	1837.7	1837.8	1837.8
0.379	1586.0	1586.1	1586.1
0.392	1417.5	1417.6	1417.6

By comparing the data of different relative error tolerances and iterations, it can be seen that more strict relative error tolerances and more iterations cannot bring more accurate results to the data. Considering that using more strict relative error tolerance and more iterations will increase the calculation time, and there is no more change to the data, the simulation results with relative error tolerance of 0.01 and iterations of 300 are still used.

The determined dissimilar error iteration data is used to analyze the temperature data of the model divided by Mesh 2 and Mesh 3. The results are shown in figs. 11 and 12.

The formation of the high-temperature fireball is formed by the oxyacetylene flame in a laboratory environment. Through the designed simulation device, the multi-pipe injection technology is adopted to form a stable high-temperature combustion-like fireball area, as shown in fig. 13.

After the flame is relatively stable, use infrared thermal imagers to collect the temperature of the fireball at this time. Two infrared thermal imagers were used to verify the temperature. One is DL700 infrared thermal imager of Dali Technology Co., Ltd. and the other is ImageIR5300 infrared thermal imager of Germany. The comparison of parameters between the two infrared thermal imagers is shown in tab. 4.

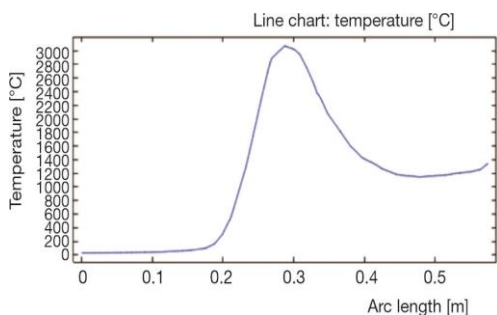


Figure 11. The second mesh temperature graph

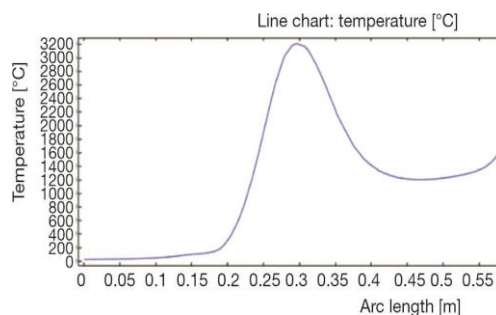


Figure 12. The third mesh temperature graph

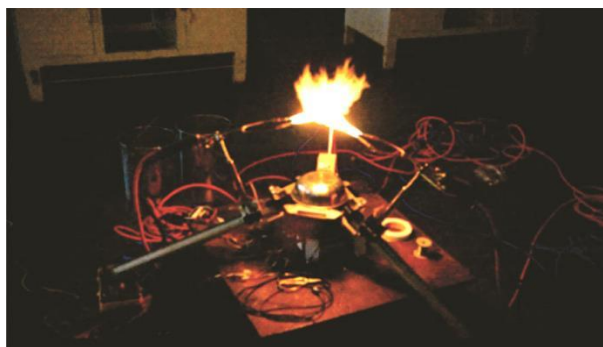


Figure 13. High temperature fireball

Table 4. Parameter comparison of infrared thermal imager

	DL700	ImageIR5300
Detection band	8-14 $\mu\text{m}$	2-5.7 $\mu\text{m}$
resolving power	640 $\times$ 480	320 $\times$ 256
Frame rate	50-60 Hz	200 Hz

When using DL700 infrared thermal imager for temperature measurement, it is difficult to display temperature distribution completely because the visualization upper limit of thermal imager is 2273.15K. Therefore, the local temperature analysis of flame can only be carried out in the docking software. Multiple images were used to analyze the results to reduce errors. The image and temperature curve are shown below, figs. 14 and 15. From the line sampling analysis in the temperature curve, it can be seen that the local temperature of the flame has exceeded 3273.15 K.

Then the temperature was measured by using ImageIR5300 infrared thermal imager under the same external parameters. The temperature images and data collected are shown below, fig. 16.

The flame image taken by imageIR5300 infrared thermal imager is also analyzed by line sampling. According to the data on L1 line segment, the maximum temperature of fireball reaches 3478.13 K, and the temperature distribution histogram also reflects the same temperature law.

The temperature at the end of the flame is unstable and difficult to collect. Therefore, in order to make an accurate comparative analysis, 11 points were selected, tab. 5, from the

numerical simulation results of the flame front after eliminating the possible influence of relative error tolerance and iteration, and the temperature data collected by DL700 infrared thermal imager and ImageIR5300 infrared thermal imager were also analyzed.

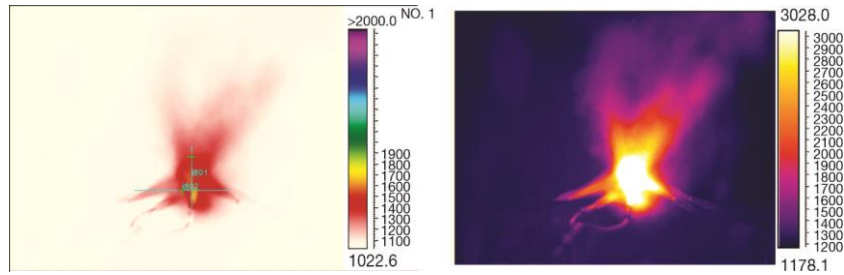


Figure 14. The DL700 infrared temperature chart

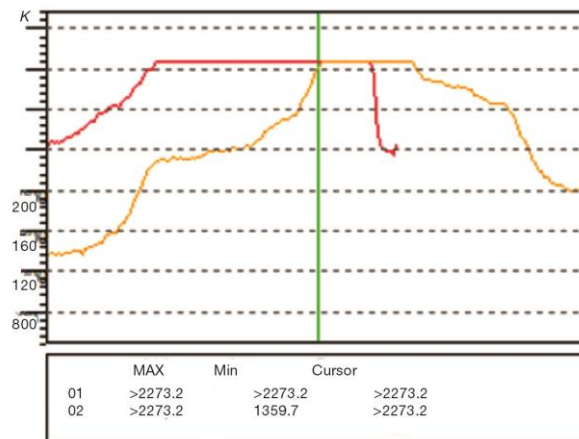


Figure 15. The DL700 infrared temperature line chart

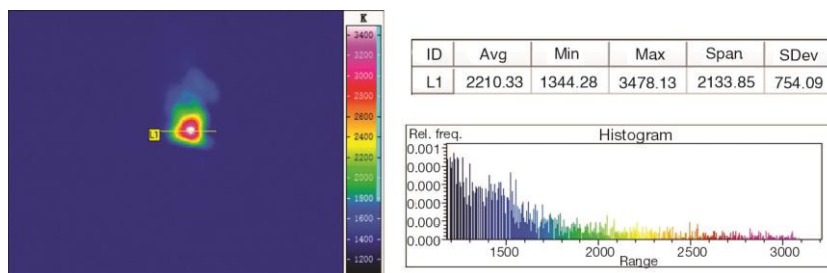
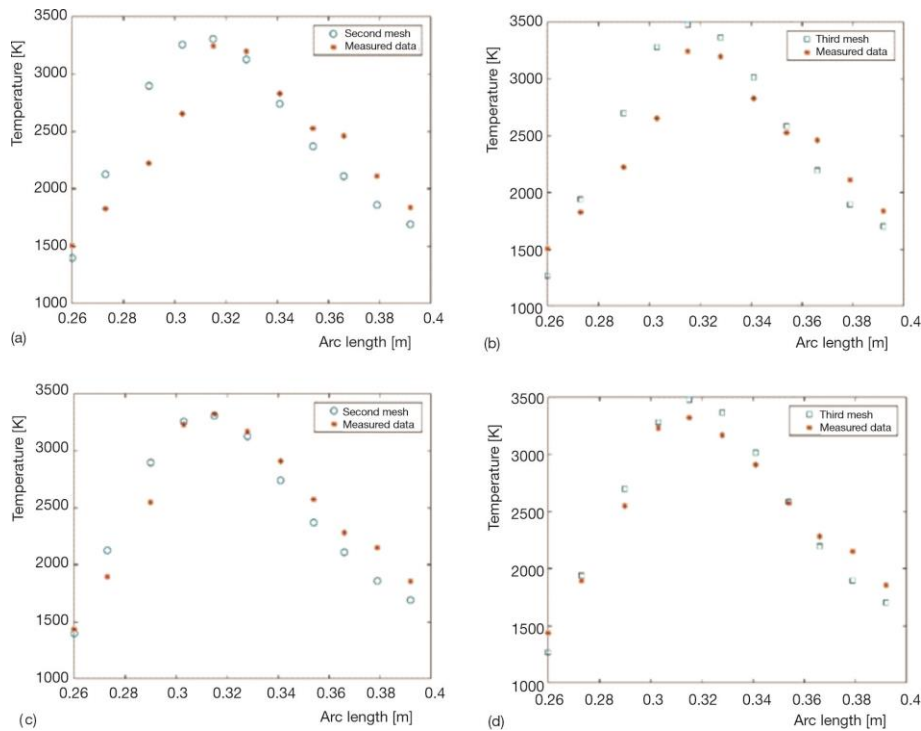


Figure 16. Temperature data diagram of ImageIR5300 infrared thermal imager

Considering the influence of the surrounding environment and the possible equipment problems of the infrared thermal imager itself, as well as the deviation between the simulation results and the actual results, there may be errors in the collected data. Calculate the temperature error according to the data of the sampling points, the collected simulated data points and experimental data points of the second mesh and the third mesh are plotted in a chart to analysis, as shown in fig. 17.

**Table 5. Temperature data**

Arc length [m]	Second mesh [K]	Third mesh [K]	DL700 [K]	ImageIR5300 [K]
0.260	1397.75	1268.85	1506.35	1436.07
0.273	2126.85	1940.95	1825.25	1894.99
0.290	2897.95	2700.05	2222.95	2547.64
0.303	3257.75	3282.95	2653.65	3231.64
0.315	3307.45	3478.15	3247.05	3324.68
0.328	3128.75	3367.35	3198.05	3169.35
0.341	2741.65	3017.55	2831.45	2912.4
0.354	2370.95	2585.35	2526.85	2575.41
0.366	2110.85	2197.05	2463.15	2283.8
0.379	1859.15	1895.15	2111.45	2151.88
0.392	1690.65	1702.65	1835.85	1856.8



**Figure 17. Data comparison chart; (a) DL700 and Mesh 2, (b) DL700 and Mesh 3, (c) ImageIR5300 and Mesh 2, and (d) ImageIR5300 and Mesh 3**

After calculation and analysis, the average error of the temperature distribution between Mesh 2 and DL700 infrared thermal imager is 10.59%, and that between Mesh 3 and DL700 infrared thermal imager is 10.27%. The average error of the temperature distribution of Mesh 2 and ImageIR5300 is 7.00%, and that of Mesh 3 and ImageIR5300 is 5.77%. ImageIR5300 has higher temperature upper limit and frame rate than DL700 infrared thermal imager, and the temperature measurement results are more reference. Although the temperature distribution trend of the two meshes is similar, the temperature distribution error of Mesh 3 is smaller than that of the two infrared thermal imagers, and the temperature curve is more accurate. Therefore, Mesh 3 is selected to divide the simulation results of calculation.

## Conclusion

In this paper, a high temperature fireball quasi-static simulation device is established for experiment. Through the experiment and numerical analysis of the high temperature fireball under the multi-pipe injection technology, a new understanding of fireball temperature is provided. The experimental data verifies the correctness of the model. Through full-scale CFD simulation and heat transfer simulation, the flow characteristics and mass fraction changes inside the fireball are determined. The numerical model was verified with an infrared thermal imager, and the changes in the temperature field of the fireball were observed. The numerical simulation results are in good agreement with the experimental results, and the error is about 5.77%, which verifies the correctness of the numerical simulation. It can be seen that the  $k-\varepsilon$  turbulence model and the solution of the heat of chemical reaction can well reproduce the actual combustion process of the high-temperature fireball. Through this numerical simulation method, a powerful verification scheme is provided for the detection of complex multiple temperature fields.

## Acknowledgment

This work was supported by the National Natural Science Foundation of China (NSFC) (No. 52075504), Fund for Shanxi '1331Project' Key Subject Construction, Guangdong Provincial Key Laboratory for Electronic Functional Materials and Devices (No. EFMD2020001Z).

## Reference

- [1] Jr, Feier, A Numerical Study of Three-Dimensional Flame Propagation over Thin Solids in Purely Forced Concurrent Flow Including Gas-Phase Radiation, Ph. D. thesis, Case Western Reserve University, Cleveland, O., USA, 2007
- [2] Cloete, S., *et al.*, An Assessment of the Ability of Computational Fluid Dynamic Models to Predict Reactive Gas-Solid Flows in a Fluidized Bed, *Powder Technology*, 215 (2012), Jan., pp.15-25
- [3] Wenqi, Z., *et al.*, DEM Simulation of Gas-Solid Flow Behaviors in Spout-Fluid Bed, *Chemical Engineering Science*, 61 (2006), 5, pp. 1571-1584
- [4] Wei, D., *et al.*, Computational Fluid Dynamics (CFD) Modeling of Spouted Bed: Assessment of Drag Coefficient Correlations, *Chemical Engineering Science*, 61 (2006), 5, pp. 1401-1420
- [5] Kamnis, S., *et al.*, Mathematical Modelling of Inconel 718 Particles in HVOF Thermal Spraying, *Surface and Coatings Technology*, 202 (2008), 12, pp. 2715-2724
- [6] Wojciech, P., *et al.*, Modeling of Particle Transport and Combustion Phenomena in a Large-Scale Circulating Fluidized Bed Boiler Using a Hybrid Euler-Lagrange Approach, *Particuology*, 16 (2014), Oct., pp. 29-40
- [7] Wang, H., *et al.*, A Comparison Between Direct Numerical Simulation and Experiment of the Turbulent Burning Velocity-Related Statistics in a Turbulent Methane-Air Premixed Jet Flame at High Karlovitz Number, *Proceedings of the Combustion Institute*, 36 (2017), 2, pp. 2045-2053
- [8] Gonzalez, F., *et al.*, CFD Modeling of Combustion of Sugarcane Bagasse in an Industrial Boiler, *Fuel*, 192 (2017), Apr., pp. 31-38
- [9] Lan, X., *et al.*, Numerical Simulation of Transfer and Reaction Processes in Ethylene Furnaces, *Chemical Engineering Research and Design*, 85 (2007), 12, pp. 1565-1579
- [10] Shunli, Z., *et al.*, Application of EDC-Model in Numerical Simulation of 3-D Combustion Flows, *Applied Science and Technology*, 32 (2005), 4, pp. 48-50
- [11] Weijie, Y., *et al.*, Experiments on Measurement of Temperature and Emissivity of Municipal Solid Waste (MSW) Combustion by Spectral Analysis and Image Processing in Visible Spectrum, *Energy & fuels*, 27 (2013), Nov.-Dec., pp. 6754-6762
- [12] Collazo, J., *et al.*, Numerical Modeling of the Combustion of Densified Wood Under Fixed-Bed Conditions, *Fuel*, 93 (2012), Mar., pp. 149-159

- [13] Gomez, M., et al., CFD Modelling of Thermal Conversion and Packed Bed Compaction in Biomass Combustion, *Fuel*, 117 (2014), Part A, pp. 716-732
- [14] Hjartstam, S., et al., Computational Fluid Dynamics Modeling of Oxy-Fuel Flames: The Role of Soot and Gas Radiation, *Energy Fuels*, 26 (2012), 5, pp. 2786-2797
- [15] Ghadamgahi, M., et al., A Comparative CFD Study on Simulating Flameless Oxy-Fuel Combustion in a Pilot-Scale Furnace, *Journal of combustion*, 2016 (2016), ID6735971
- [16] Khare, S. P., et al., Factors Influencing the Ignition of Flames from Air-Fired Swirl Pf Burners Retrofitted to Oxy-Fuel, *Fuel*, 87 (2008), 7, pp. 1042-1049
- [17] Wang, A. H., et al., Numerical Simulation of Combustion Characteristics in High Temperature Air Combustion Furnace, *Journal of Iron and Steel Research International*, 16 (2009), 2, pp. 6-10
- [18] Liu, C., et al., Effects of Five Different Parameters on Biodiesel HCCI Combustion in Free-Piston Engine Generator, *Thermal Science*, 25 (2021), 6A, pp. 4197-4207
- [19] Samal, B. S., et al., Influence of Turbulence on the Efficiency and Reliability of Combustion Chamber of the Gas turbine, *Thermal Science*, 25 (2021), 6A, pp. 4321-4332
- [20] Kun, L., et al., A Computational Method to Solve for the Heat Conduction Temperature Field Based on Data-Driven Approach, *Thermal Science*, 26 (2022), 1A, pp. 233-246
- [21] Wang, M., et al., Numerical Simulation on the Emission of NOx from the Combustion of Natural Gas in the Sidewall Burner, *Thermal Science*, 26 (2022), 1A, pp. 247-258
- [22] Xie, K., et al., Numerical Study on Flame and Emission Characteristics of a Small Flue Gas Self-Circulation Diesel Burner with Different Spray Cone Angles, *Thermal Science*, 26 (2022), 1A, pp. 389-400
- [23] Ban, Q., et al., Brazing Technology and Common Problem of Refrigeration and Air-Conditioning System, *Refrigeration and Air-Conditioning*, 9 (2009), 4, pp. 98-100
- [24] Vazquez, M., et al., The Robustness Issue on Multigrid Schemes Applied to the Navier-Stokes Equations for Laminar and Turbulent, Incompressible and Compressible Flows, *International Journal for Numerical Methods in Fluids*, 45 (2004), 5, pp. 555-579
- [25] Wilcox, D. C., *Turbulence Modeling for CFD*, DCW Industries, Lake Arrowhead, Cal., USA, 2006
- [26] Magnussen, B. F., et al., On Mathematical Modeling of Turbulent Combustion with Special Emphasis on Soot Formation and Combustion, *Symposium on Combustion*, 16 (1977), 1, pp. 719-729